Check for updates

Sugar based cationic magnetic core–shell silica nanoparticles for nucleic acid extraction†

Tammar Hussein Ali, [ID] *ab Amar Mousa Mandal,c Thorsten Heidelberg [ID] *d and Rusnah Syahila Duali Hussen d

Nucleic acid (NA) extraction is an essential step in molecular testing for a wide range of applications. Conventional extraction protocols usually suffer from time consuming removal of non-nucleic acid impurities. In this study, a new magnetic nanoparticle (MNP) is presented to simplify the NA extraction. A core–shell design, comprising of a ferromagnetic core coated with mesoporous silica, forms the basis of the functional nanoparticle. Chemical functionalization of the silica coating includes a multistep synthesis, in which an activated nanoparticle is coupled with a triethylene glycol spaced glycosyl imidazole. The molecular design aims for charge interactions between the imidazolium-based positive nanoparticle surface and nucleic acids, with specific hydrogen bonding between the surface bonded carbohydrate and nucleic acid targets to ensure nucleic acid selectivity and avoid protein contamination. Two different carbohydrates, differing in molecular size, were selected to compare the efficiency in terms of NA extraction. A triethylene glycol spacer provides sufficient flexibility to remove particle surface constraints for the interaction. The Brunauer–Emmett–Teller (BET) analysis shows a significantly larger surface area for the disaccharide-based particles NpFeSiImMalt ($\sim$181 m^2 g^{-1}) compared to the monosaccharide analogue NpFeSiImGlc ($\sim$116 m^2 g^{-1}) at small particles sizes (range $\sim$ 15 nm) and sufficient magnetization (29 emu g^{-1}) for easy isolation by an external magnetic field. The particles enabled a high DNA particle loading ratio of 30–45 wt% (MNP/DNA ratio), reflecting an efficient extraction process. A high desorption rate (7 min) with more than 86% of unchanged DNA loading was recorded, indicating low damage to the target extract.

Introduction

In the last decade, the synthesis of nanoparticles was mainly focused on the application of traditional materials science catalysts,[1,2] optical coating,[3,4] and ceramics.[5] But in the past few years, due to advancements in the synthesis and characterization of nanomaterials, their application has experienced rapid developments. Among various materials with cheaper and the simple synthesis process is magnetic materials, which can be prepared using numerous synthetic methods such as[6–8] classical co-precipitation,[9] hydrothermal reaction,[10] sol–gel synthesis,[11] thermal decomposition,[12] microemulsion synthesis,[13]

sonochemical reaction,[14] electrospray synthesis,[15] and laser pyrolysis.[16] A large scale synthesis was achieved using the co-precipitation method to prepare iron oxide NPs by aging a stoichiometric mixture of inorganic salts in basic aqueous media and controlling the aging condition. However, these magnetic materials with particle size smaller than 100 nm have been intensively used in many technology applications, among others,[1,17–30] although the fabrication of their surface with appropriate coating and functional groups or molecules are desired for good performance coupled with target agents. Especially, the core–shell fabrication will prevent the multistep conjugations to a single component NP as well as avoid conjugated different molecules and low loading on the NP surface, which may interfere with targeting capabilities.[8] The mesoporous silica core–shell is considered as a very promising route due to some good properties like biocompatibility, excellent stability, nontoxicity, and ease of conjugation with various functional groups, which enable the coupling and labeling of biotargets with selectivity and specificity.[31–33] The synthesis of core–shell magnetic nanoparticles conjugated with biocompatible and degradable materials like carbohydrates is useful for separation and drug delivery, which can be driven and controlled under an external magnetic field.

Faculty of Pharmacy, Department of Pharmaceutical Chemistry, Al-Muthanna University, 66001 Samawah, Al Muthanna, Iraq. E-mail: tammar86@gmail.com; tammar@mu.edu.iq

bMolecular Design and Synthesis, Department of Chemistry, KU Leuven, Celestijnenlaan 200F, 3001 Leuven, Belgium

cCollege of Basic Education, Science Department, Al-Muthanna University, 66001 Samawah, Al Muthanna, Iraq

dChemistry Department, Faculty of Science, University of Malaya, 50603 Kuala Lumpur, Malaysia. E-mail: heidelberg@um.edu.my

To date, the greatest advances have been achieved in the fabrication of magnetic nanoparticles in order to reduce the possibility of getting agglomeration and sustain their desired properties.[34] However, different coating materials have been investigated with different inorganic and organic and materials and are still ongoing. For example, the functionality of dextran-coated monocrystalline[35] and cross-linked iron nanoparticles[36] have been reported by Weissleder. Bae *et al.* (2010) developed chitosan coated oligosaccharide stabilized ferrimagnetic iron oxide nanocubes.[37] Häfeli *et al.* (2009) used polyethylene oxide coated MNPs.[38] Also, polyvinyl alcohol-coated MNPs[39] and poly(lactide-*co*-lycolide) (PLGA) have been reported as approved polymer coating materials for a variety of drug delivery systems.[40] The latter fabrication was focused on surface silanization (core–shell or/and coated) of MNPs due to several advantages and impart functionalized groups over the surface of bare MNPs to maintain several properties. During the last twenty years, several research works have been gaining attention, such as those of Wu *et al.* (2008), who synthesized silane-coated MNPs with hydroxyl groups present on the surface of MNPs, which later reacted with methoxy groups of the silane molecules to form Si–O bonds while leaving the exposed terminal group for the attachment of other molecules.[41] Qiang Ma *et al.* (2012) reported the synthesis of core–shell MNPs by a controlled reverse microemulsion method.[42] Chandekar *et al.* (2021) described the synthesis of core–shell magnetic nanoparticles (NPs) consisting of poly acrylic acid (PAA) coated cobalt ferrite (CF) also *via* the co-precipitation route,[43] although the principal choices for coated magnetic nanoparticles with silica are Stöber method and sol–gel method.[44] Naeimi *et al.* (2013), Halilu *et al.* (2016), and Lu *et al.* (2021) prepared core–shell MNPs by a simple and low cost co-precipitation method using ammonia-catalyzed hydrolysis of TEOS.[21,45,46] In this work, the synthesis of tetraethyl orthosilicate Fe_2O_3 magnetic core–shell silica immobilized with sugar as a strong hydrophilic group leads to the development of an efficient, stable, and low toxicity material. Moreover, there are advantages of incorporating sugar that has several properties like biocompatibility, high charge density, ability to improve dissolution, and low toxicity.

One of the main challenges in the biotechnology field is the isolation and purification of highly purified forms of various biomolecules like antibodies, antigens, nucleic acids, and DNAs, which are usually desired for numerous genetic and molecular studies.[47–49] Several bio-separation techniques have been introduced to achieve the separation in resource limited regions, and among them, the magnetic separation appears as a potential candidate to be employed, which can be considered as a simple process, robust and versatile in operation by applying magnetic force[44,50].

In comparison with our previous report,[51] the replacement of the hydrophobic alkyl chain by a large hydrophilic structure with capabilities of acting as acceptors or donors in the formation of hydrogen bonds will significantly enhance and strengthen the interaction with biomolecules due to the multiple number of hydrogen bonds, which totally will have a sizable effect. Although the bond strength of the hydrophobic bond equal to $\sim$1 kcal mol^{-1} which is lower than the hydrogen bond ($\sim$7 kcal mol^{-1}).[52] In addition, the surface area of interaction will increase especially when di-saccharide is used in comparison with the alkyl chain.

Since the surface of the magnetic nanoparticles is a key factor for the extraction, a new design of fabricated MNP is achieved, containing highly interactive hydrophilic biocompatible (sugar) and cation (imidazole) molecules with triethylene glycol as a dispersant to increase the distance between these two interacting sources. The particle has been shelled with silicate using tetraethyl orthosilicate (TEOS) and phase transfer reagents (3-chloropropyl-triethoxysilane (CPTES)) to further provide nucleation sites for the subsequent silica coating. This paper first outlines the synthesis of composite MNPs and then discusses the characterization applied for surface modification. Finally, the potential applications of these immobilized particles in the extraction of DNA are highlighted and demonstrate the greater DNA adsorption capability of the MNPs.

Materials and characterization

The chemical reagents and solvents were purchased from various commercial sources and used without purification. TLC (thin-layer chromatography) was checked on pre-coated plates of silica gel 60 (GF254) with sulfuric acid–ethanol solution (configured with 10 mL of sulfuric acid and 90 mL of ethanol) for visualization. Purification of synthesis compounds was done by applied column chromatography on silica gel 35–60 mesh using the flash technique. IR spectra were recorded on a Perki-nElmer Frontier ATR FT-IR spectrometer. Dried nanoparticles were subjected to thermal gravimetric and differential thermal analysis (TG-DTA) with 20 °C min^{-1} ramping. Transmission electron microscopy (TEM) was performed with an FEI Tecnai G2-F20 operating at 200 kV with 0.2 nm resolution. Samples were prepared by dispersing the nanoparticles in ethanol and sonicated for 5 min prior to deposition on an amorphous carbon-coated 300 mesh copper grid before allowing the solvent to evaporate. The surface morphology of the samples was analyzed by a field emission scanning electron microscope (SEM) on a Hitachi SU8200 equipped with an energy dispersive X-ray spectrometer EDX (QUANTAX FlatQUAD, Bruker AXS) operated at an accelerating voltage of 20 kV and a working distance of 13 mm. A few milligrams of the dried sample were added into a FESEM cell and subsequently scanned by the electronic microscope. The XRD pattern of the particles was recorded on a Bruker D8 Advance X-ray diffraction AXS using Cu Kα radiation ($d = 1.54$ Å) at a voltage of 40 kV and current of 40 mA at ambient temperature. The magnetic properties were investigated by using a Lakeshore 7400 series, 7407 model with 7 inch electromagnet vibrating sample magnetometer (VSM). The nitrogen adsorption porosimetry was carried out on a surface area analyzer (micromeritics ASAP 2020). The analysis was conducted at room temperature in a field of ±10 kOe. Structural identities using ^{1}H NMR and ^{13}C NMR spectra were obtained on a Bruker AVN-400 MHz spectrometer.

Synthesis of silyl propyl-*H*-imidazole functionalized magnetic nanoparticles NpFeSiIm

The particles were synthesized by dispersing the precursor NpFeSiCl (2.0 g) (the preparation of this particle was carried out according to our previous report[51]) in 20 mL of toluene, and subsequently, a well dissipated triethyl amine (4.6 g, 45.46 mmol, 1.5 eq.) was added. The reaction mixture was stirred at 600 rpm for 30 min at room temperature before excess imidazole (2.0 g, 29.38 mmol) was added. Then, the reaction was vigorously stirred at 100 °C for 24 h. The resulting NpFeSiIm was separated by centrifugation at 4000 rpm speed and washed with deionized water repeatedly and finally with acetone and dried at 40 °C for 6 h to give 2.8 g of dark brown colored product.

Preparation of 2-(2-(2-hydroxyethoxy)ethoxy)ethyl toluenesulfonate (3)

Compound **3** was prepared according to the literature with some modifications.[53,54] To a solution of 30 mL of triethylene glycol in dichloromethane (DCM) (50 mL) was added tosyl-Cl (5.0 g, 26 mmol), and the reaction mixture was stirred at 0 °C before triethyl amine (Et$_3$N) (5.3 g, 52 mmol) was added drop-wise. After stirring overnight at room temperature, the mixture was extracted with aqueous sodium bicarbonate (NaHCO$_3$ aq.) and DCM three times. The combined organic phase was dried over magnesium sulphate (MgSO$_4$) and concentrated to provide monotosyl triethylene glycol as colorless oil (7.6 g, 95% yield). The product was almost pure and subjected to the next reaction without further purification.

^{1}H NMR (400 MHz, CDCl$_3$) δ = 7.74, 7.30 dd (4H, Ar); 4.09 m (2H, C$\underline{H_2}$ OH); 3.64–3.50 m (10H, OCH$_2$); 2.38 s (3H, CH$_3$–tosyl).

General procedure of glycosylation

The reaction was carried out according to similar reported methods.[55–58] To a solution of β-sugar peracetate (4.0 mmol) (glycose pentaacetate or maltose octaacetate) in DCM (40 mL) 2-(2-(2-hydroxyethoxy)ethoxy)ethyl toluenesulfonate (**3**) (0.73 g, 2.4 mmol) was added, and the solution was treated with BF$_3$ × OEt$_2$ and stirred at room temperature for 3 h. The reaction mixture was extracted with NaHCO$_3$ aq. and subsequently dried over MgSO$_4$. The purification of the crude product included column chromatography using hexane and ethylacetate.

2-[2-(2-Toluene-4-sulfonyloxy)ethoxy]ethoxyl-2,3,4,6-tetra-*O*-acetyl-β-D-glucopyranoside (5). Glucose pentaacetate (1.56 g, 4.0 mmol) was reacted with 2-(2-(2-hydroxyethoxy)ethoxy)ethyl toluene sulfonate (**3**) (1.46 g, 4.8 mmol) according to the general glycosylation procedure and purified by column chromatography with eluent hexane : ethyl acetate 3 : 2 to yield compound **5** as a brown oil (1.8 g, 71%). ^{1}H NMR (400 MHz, CDCl$_3$) δ = 7.72, 7.29 dd (2H, Ar); 5.13 t (H-3); 5.00 t (H-4); 4.90 t (H-2); 4.55 d (H-1); 4.20 dd (H-6a); 4.08–400 m (5H, H-6b, α-OCH$_2$, OCH$_2$ of AcOEt solvent remain); 3.87–3.82 m (H-5); 3.67–3.48 m (10H, OCH$_2$); 2.37 s (3H, CH$_3$tosyl); 2.03–1.92 m (12 + 3H, Ac$_{Glc}$, Ac remain solvent); 1.17 t (3H, CH$_3$ solvent). $^3J_{1,2}$ = 8.1; $^3J_{2,3}$ = 8.1; $^3J_{3,4}$ = 9.4; $^3J_{4,5}$ = 9.5; $^3J_{5,6a}$ = 4.06; $^2J_6$ = 12.2 Hz. ^{13}C NMR (CDCl$_3$) δ = 170.53, 170.10, 169.38, 169.29 (CO); 144.80, 132.88 (2× C–Ar); 129.81, 127.89 (2× CH–Ar); 100.71 (C-1); 72.73 (C-4); 71.64 (C-2); 71.18 (C-3); 70.62, 70.52, 70.20, 69.26, 69.26, 68.60 (6× OCH$_2$); 68.32 (C-5); 61.85 (C-6); 21.53, 20.93, 20.64, 20.57, 20.52 (Ac).

2-[2-(2-Toluene-4-sulfonyloxy)ethoxy]ethoxyl-2,3,6,2′,3′,4′,6′-hepta-*O*-acetyl-β-D-maltopyranoside (7). Maltose octaacetate (2.71 g, 4.0 mmol) was reacted with 2-(2-(2-hydroxyethoxy)ethoxy)ethyl toluene sulfonate (**3**) (1.46 g, 4.8 mmol) according to the general glycosylation procedure and purified by column chromatography with eluent hexane : ethyl acetate 2 : 1 to yield compound **7** as a colorless oil (2.0 g, 54%). ^{1}H NMR (400 MHz, CDCl$_3$) δ = 7.77, 7.33 dd (4H, Ar); 5.38 d (H-1′); 5.33 t (H-3′); 5.22 t (H-3); 5.02 t (H-4′); 4.84–4.77 m (2H, H-2, H-2′); 4.59 d (H-1); 4.48, 4.44 dd (H-6a); 4.21 td (2H, H-6b, H-6′b); 4.13 m (2H, H-4, H-6a); 3.98 (H-5′); 3.69–3.53 m (10H, OCH$_2$); 2.42 s (3H, CH$_3$–tosyl); 2.03–1.92 m (12 + 3H, Ac$_{Maltose}$). $^{1,3}J_{1,2}$ = 8; $^{1,3}J_{1′,2′}$ = 3.9; $^{1,3}J_{2′,3′}$ = 12; $^{1,3}J_{3,4}$ = 9; $^{1,3}J_{4′,5′}$ = 9.8; $^{1,3}J_{5,6a}$ = 2.4; $^2J_{6b}$ = 11.8; $^2J_{6′b}$ = 11.8. ^{3}C NMR (CDCl$_3$) δ = 170.56, 170.54, 170.21, 169.95, 169.70, 169.45 (CO); 144.83, 132.90 (2× C–Ar); 129.86, 127.95 (2× CH–Ar); 100.29 (C-1); 95.50 (C-1′); 75.31 (C-3); 72.74 (C-4); 72.48 (OCH$_2$–tosyl); 72.07 (C-4′); 70.70, 70.68, 70.56, 70.21 (OCH$_2$); 69.98 (C-2); 69.29 (C-5); 69.27, 69.19, 69.11, 68.67, 68.63 (5× OCH$_2$); 68.42 (C-2′); 67.97 (C-5′); 62.77 (C-6); 61.64 (C-6′); 21.62 (CH$_3$–tosyl); 20.89, 20.83, 20.67, 20.63, 20.59 (Ac).

General procedure of synthesis of sugar imidazolium based magnetic nanoparticle (NpFeSiImSugaracetate)

Imidazole functionalized magnetic nanoparticles (1.0 g) were dispersed in MeCN (50 mL) and ultrasonicated for 20 min. Sugar tosyl **5** or **7** (1.0 g) was added, and the reaction mixture was stirred at 55 °C for 2 days. After cooling to room temperature, the product was isolated by magnetic decantation. It was washed with acetone (3 × 20 mL), and dried for 6 h at 45 °C to provide NpFeSiImSuageacetate (1.3–1.5 g) as a dark brown solid.

General procedure of deacetylation of NpFeSiImSuage

A mixture of the protected sugar magnetic particles in methanol was treated with a catalytic amount of sodium methoxide (NaOMe), and the reaction was kept at room temperature for 6 h. The catalyst was removed by treatment with acidified methanol (0.1 M HCl in 3 mL) and the particles were isolated by magnetic decantation, washed with acetone (3 × 20 mL), and dried for 6 h at 45 °C to provide NpFeSiImSugar as dark brown solid.

Extraction of DNA from blood and attachment with particles

The preparation of the DNA–nano complex was carried out similar to our previous report[51] by dissolving a genomic DNA with different weight ratios of magnetic NP ranging from 300–1200 μg in nuclease-free water. The extraction was done by transferring 300 μL of whole blood to 1.5 mL tube containing 900 μL RBC lysis solution. It was mixed by vortexing and subsequently incubated for 5 min at room temperature and centrifuged at 13 000 rpm for 1 min. The supernatant was

removed by retaining the white cell pellet and 20 μL of proteinase K and 300 μL of BB3 (cell lysis solution) were mixed inside a micro-centrifuge tube by vortexing for 15 s and subsequently incubated at 56 °C for 15 min. 1.5 μL RNase solution was added to the cell lysate and incubated at 37 °C for 15–30 min, the mixture was chilled to room temperature, and then 100 μL PPT (protein precipitation buffer) was added to the cell lysate and vortexed vigorously at high speed for 20 s.

The weight ratios of magnetic NP to DNA range from 15, 30, 45 to 60, DNA (20 μg mL^{-1}). The mixture was vortexed and incubated for 15 min at 4 °C to allow the formation of the carrier/DNA complex. The nanomaterial with DAN attached was collected by magnetic separation, and the rest of the lysate content was discarded. 1 mL of 70% ethanol was added to the DNA nanoparticle, and pipetting was done up and down several times to wash the DNA nanoparticle. The nano-material with DNA attached was collected after washing by applying an external magnetic field, and the rest of the solution was discarded. This step was repeated one more time to ensure that the DNA molecules were washed perfectly. Electrophoresis (1% agarose gel) was applied at 110 V for 15 min in TBE buffer in order to confirm the binding. The band was stained with ethidium bromide (EthBr) included in the agarose gel. The resulting migration patterns were visualized under UV irradiation (G-BOX, SYNGENE). The optimum ratio of NpFeSiImSugar/DNA was found to be 30 and 45 for glycose and maltose particles immobilized, respectively.

DNA release

The dissociation of NpFeSiImSugar/DNA complex was carried out by adding 50 μL of elution buffer AW1, which contains a high concentration of chaotropic salt and is incubated at 65 °C for 5 min. The mixture was vortexed until the pellet was (visually) completely re-suspended and then centrifuged for 30 s at approximately 14 000 rpm. The spin column (containing silica membrane) was applied for the supernatant. The resulting DNA was purified by washing twice with buffer (containing absolute ethanol) and then centrifuged for 1 min at 14 000 rpm. After that, the nanoparticles were removed from the silica to the collection tube, the DNA filament was attached to the silica membrane, and then the membrane containing the DNA was dried from ethanol by re-centrifugation for 3 min at 14 000 rpm. Finally, 60 μL of elution buffer was added to the center of the spin column tube, and it was centrifuged for 1 min at 14 000 rpm to produce a purified DNA, which was stored at 4 °C until use. The DNA concentration was verified by agarose gel electrophoresis.

DNA stability

NpFeSiImSugar/DNA complex was suspended in buffer and exposed to ultrasound. The sample was aligned at the focus of a 60 kHz single-element ultrasound transducer (model Wise Clean) in a tank containing deionized water at 30 °C for periods ranging from 0 to 160 s. Electrophoresis (1% agarose gel) was then carried out at 110 V for 15 min in TBE buffer to determine whether the DNA had been structurally damaged or not. The band was stained with EthBr included in the agarose gel.

Results and discussion

Particle synthesis

Scheme 1 represents the synthesis of ionic magnetic nanoparticles based on sugar using a multistep strategy. The particles were synthesized by a chemical co-precipitation of ferrous and ferric ions in aqueous ammonia (pH 9) at a stoichiometric ratio of 3 : 2, as described by our previous work.[51] To avoid possible oxidation or aggregation of the particles and provide active surface functionalization, a SiO_2 coating was carried out according to a modified Stöber method, which was obtained by the hydrolysis of TEOS.[59–61] The further functionalization of silica coating with chloride by treatment with CPTES, which is used as the phase transfer reagents to further provide nucleation sites for the subsequent silica coating by incorporation with imidazoles in order to be a source of positive charges on the nanoparticle surface. Next, it was subjected to the final coupling with ethylene glycol sugar derivatives to provide ionic magnetic core–shell based sugar nanoparticles. The triethylene glycol acts as a dispersant to increase the distance between nanoparticles and the hydrophilic head (sugar), further inhibiting the solid-state quenching of the particles.
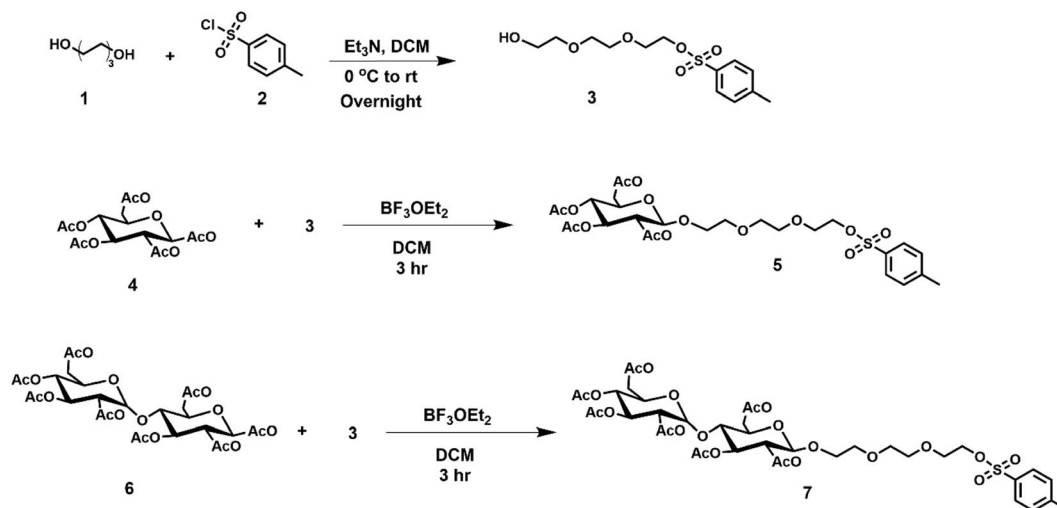
Nanoparticle characterization

The crystalline structure of sugar based magnetic core–shell nanoparticles was identified by X-ray diffraction (XRD) pattern, as shown in Fig. 1. The precursor magnetic core–shell (NpFeSi and NpFeSiCl) is identified as a combination of hematite (Fe_2O_3) and quartz (SiO_2) according to our previous report.[51] However, the phase particles of NpFeSiIm and NpFeSiImSugar (sugar = glycose and maltose) are similar to each other, which show diffraction peaks at 30.4, 35.7, 43.2, 53.5, 57.3, and 62.9°. These correspond to Fe_2O_3 on the (211), (122), and (214) crystallographic planes, respectively (PDF ref. code: 033-0664), while the SiO_2 diffractions reflect the (111), (102), (110), and (202) crystallographic planes (PDF ref. code: 033-1161). The sharp diffraction peaks indicate high crystallinity and particle sizes in the upper nano-range.
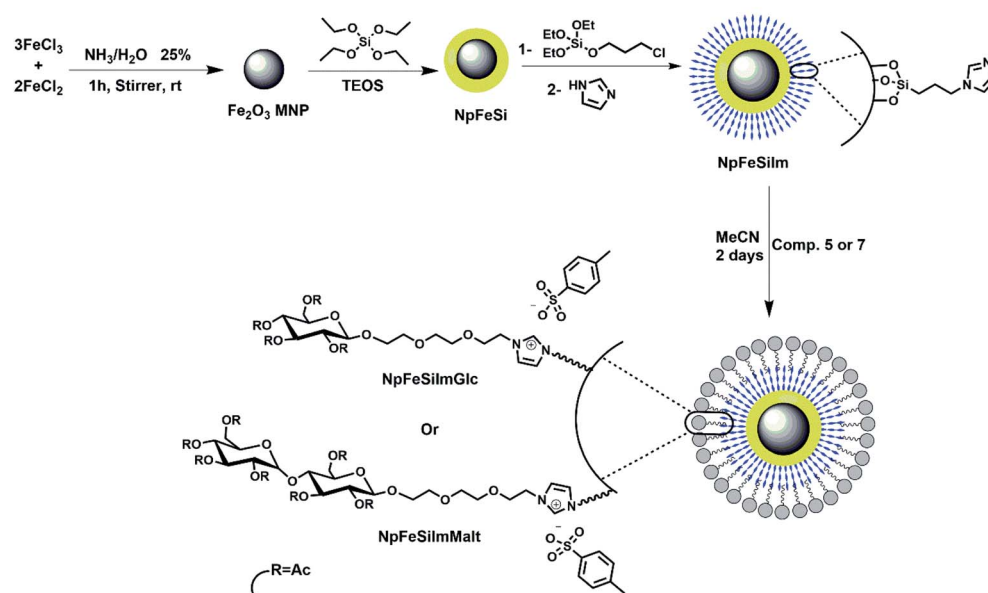
High resolution transmission electron microscopic (HRTEM) images of NpFeSiImSugar are shown in Fig. 2. The atomic structure and morphology of the nanoparticles with the lattice fringes of the magnetic core are clearly observed. The estimated lattice d-spacings were found to be ~0.22, 0.27, and 0.3 nm, which correspond to (102), (110), (202), and (111), respectively. The estimated average diameters are in the range of 5–12 nm, which appear to differ in size. These variations in the size are attributed to the agglomeration of the particles as well as due to magnetostatic interactions, which increase in the dry sample, leading to ordering and self-assembly.[62]

SEM was employed to capture the detailed morphologies of the NpFeSiImSugar, as seen in Fig. 3. The modified magnetic nanoparticles show a rough surface with spherical agglomerates in a regular pattern. By virtue of the magnetic material

Scheme 1 Synthetic pathways for the ionic magnetic core–shell nanoparticles-based sugar. (A) Synthesis of sugar tosyl. (B) Synthesis of NpFeSiImSugar.

present, the relatively uniform size distribution cannot be confirmed due to magnetic electrostatics, which assembles isolated particles.

The energy dispersive X-ray microscopy (EDX) was applied on the nanoparticles to estimate elemental composition. The analysis of particles NpFeSi and NpFeSiCl have been reported previously.[51] However, the analysis of particles NpFeSiIm and NpFeSiImSugar is displayed in supplementary Fig. S6.† The absence of chloride ions in parallel with the presence of the new element nitrogen is an indication of the successful

incorporation of imidazole on NpFeSiCl, and this is reflected in the decreasing ratio of Si and Fe to be approximately half in comparison with the precursor (Si = 6.13%, Fe = 36.72 in NpFeSiCl compared to Si = 2.85%, Fe = 19.85% in NpFeSiIm). It is clear from the elemental radiation maps that there is almost a homogeneous activation of the particle surface.

After anchoring sugar molecules on the particles, a significant change in the ratio of Fe, N, and C elements was observed, which is considered as a good indication of successful incorporation. There is almost no change in silicon ratio, indicating
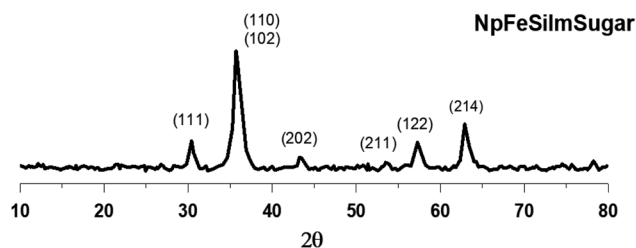
Fig. 1 XRD patterns of sugar based magnetic core–shell nanoparticles.

the hard core–shell structure. The well covered of magnetic nanoparticles (Fe_2O_3) core by the silica shell followed by carbohydrate moieties could be the reason for mismatching the actual ratio of ferric element due to brevet dispersive X-ray being in the deeper of particle and thus the reflection ratio are incorrect. However, the comparison of the elemental radiation maps suggested a homogeneous activation of the particle surface.

The thermogravimetric analysis (TGA) was used for a quantitative analysis of the anchoring of organic contents on the magnetic particle surface, in addition to determining and measuring the thermal stability of the particles. Basically, an easier analysis was provided by mathematical data-processing with differential thermogravimetry (DTG) spectra.

The TGA-DTG curves of NpFeSiIm (figure attached in ESI S7†) showed a major characteristic decomposition stage at 200 °C with a mass loss of 0.88 mg, 15.86%, which could be assigned to the physisorbed water inside the nanoparticle matrix or/and further condensation of the hydroxyl group of silica shell Q^3 $(Si(OSi)_3(OH))$ to result in Q^4 $(Si(OSi)_4)$. The latter has disappeared after the fabrication of magnetic nanoparticles with the sugar group since its exposure to reflux (heating) condition for two days, which allows the condensation to happen. One additional region of mass loss appeared at 270–450 °C (0.71 mg, 12.86%), which was attributed to the decomposition of the chloropropyl group attached to imidazole and silica. The triethylene glycol sugar functionalized nanoparticles exhibited one major peak at 450 °C, probably reflecting the
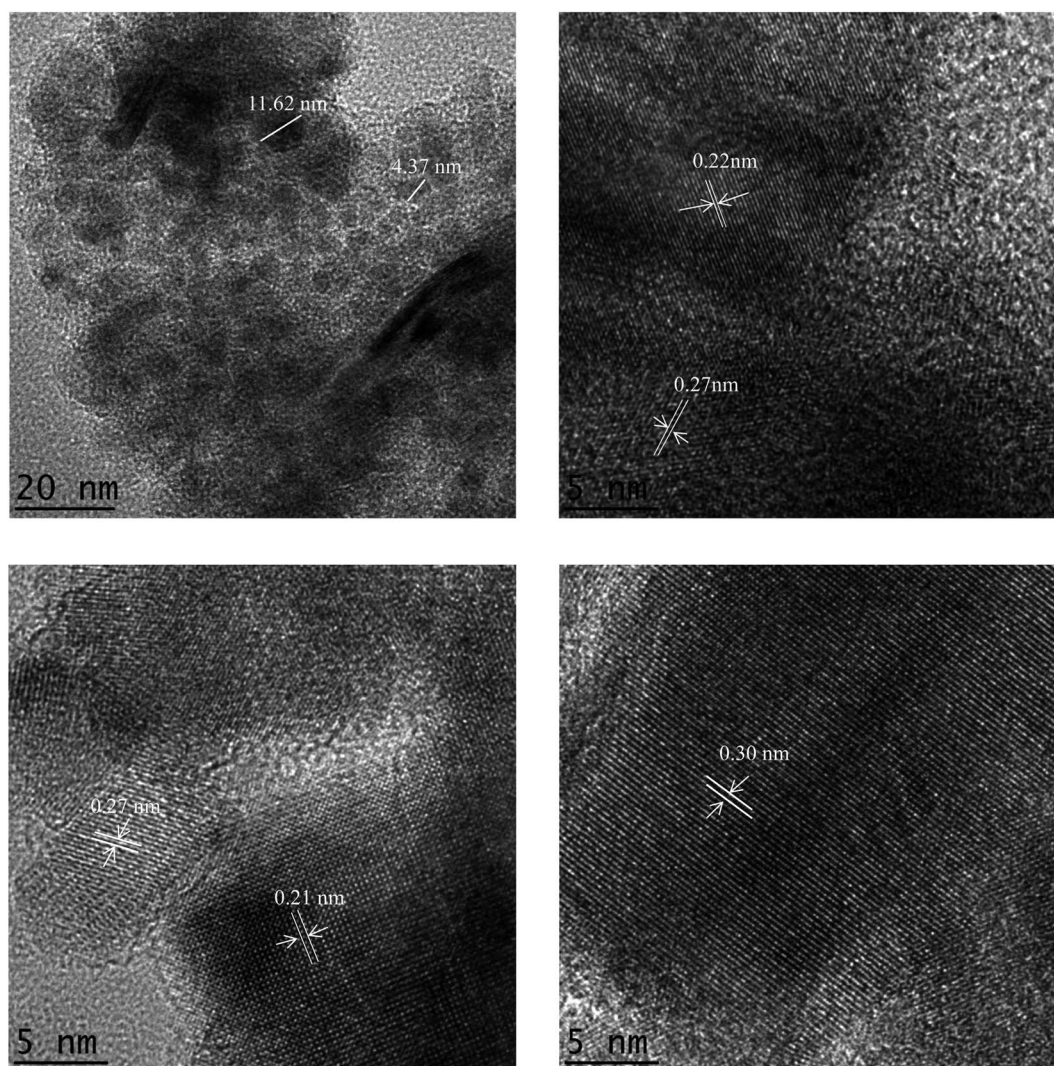

Fig. 2 HRTEM images of NpFeSiImSugar nanoparticles with lattice fringes and the particle size.
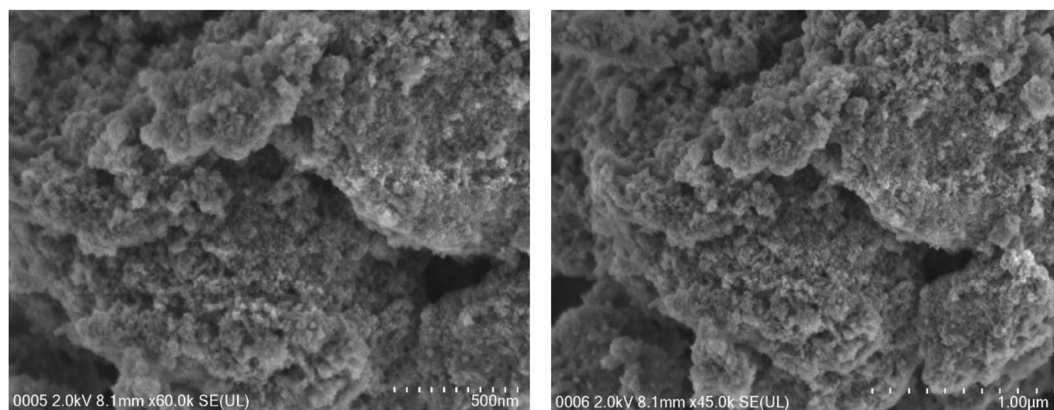
Fig. 3 FESEM images of NpFeSiImSugar.

degradation of the imidazolium glucose with a mass loss of 1.12 mg, 23.94% (Fig. 4). Two peaks were found for maltose functionalized particles around 330 °C (1.38 mg, 31.76%), which could be attributed to the dissociation of imidazolium from sugar (Fig. 4). The second mass loss at around 600 °C (0.38 mg, 21.63%) reflects the decomposition of maltose. As a result, the conclusion was that the glucose functionalized particle has more thermal stability than the maltose functionalized particle, but this does not reflect the interaction activity properties.

Magnetic anisotropy properties reflect one of the attractive features of the material, which is significantly different from conventional nanoparticles. The magnetic properties of NpFeSiImSugar nanoparticles were investigated at room temperature as a function of the magnetic field (H). The analysis of the magnetic property for the precursors NpFe, NpFeSi, and NpFeSiCl was reported in previous studies.[51,63,64] The saturation magnetization (M_s) of the nanoparticles was found to be 29 emu g^{-1}, as shown in Fig. 5. This value is similar to what was recorded for NpFeSiCl, which is an indicator for the successful immobilization of magnetic nanoparticles. The magnetization relates to a coercivity of 33 G, which is higher than the 27.2 G for NpFeSiCl, meaning the sugar particles offer high resistance to

changes in the magnetization field than the precursor. Very small hysteresis loops were observed for NpFeSiImSugar nanoparticles at a low magnetic field with weak remnant magnetization (M_r) of 1.73 emu g^{-1}. These values are conspicuously characteristic of the super-paramagnetic behavior of the nanoparticles.

The monitoring of the immobilization of surface magnetic particles was also done by IR-spectroscopy. The spectra in Fig. 6 reveal the organic chemical structure of NpFeSiIm and NpFeSiImSugar and a spectrum for precursor NpFeSiCl for a comparison. Typically, the intense and broad absorption above 3300 cm^{-1} reflects the remaining hydroxyl groups on the particle surface, and the stretching vibration band for the aliphatic CH$_n$ group was observed slightly below 3000 cm^{-1}. These absorptions increased upon the introduction of sugar molecules. The band at 1643 cm^{-1} could be assigned to the bending vibration of trapped water molecules within the silica matrix.[18] The latter disappeared after grafting of sugar molecules and reflux for two days. The absorption peak at 1253 cm^{-1} was assigned to the Si–C stretching vibration, while the bands at 1073 and 1053 cm^{-1} were attributed to Si–O–Si stretching vibrations. These values confirm the formation of the amorphous silica matrix.[19] All the NpFeSiImSugar with different
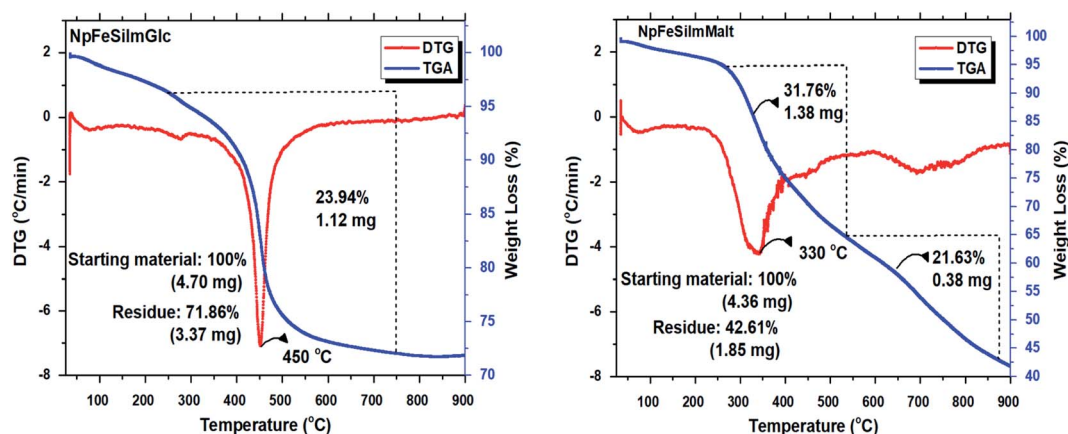

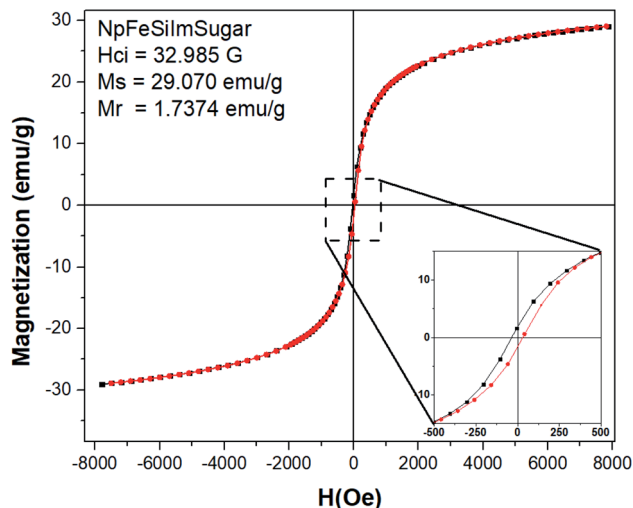**Fig. 4** TG-DTA analysis of magnetic NpFeSiImGlc and NpFeSiImMalt.

Fig. 5 Super-paramagnetic hysteresis loop for NpFeSiImSugar nanoparticle.

sugar types shows almost similar IR spectra. As a result, this FT-IR analysis gives a good indication of the presence of a silica matrix that serves as a shell to the core magnetite (Fe_2O_3) and is able to reveal the successful functionalization of the particles.

Nitrogen adsorption–desorption analysis

The nitrogen adsorption isotherms obtained for the precursor (NpFeSi and NpFeSiIm) and sugar based magnetic core–shell nanoparticles (NpFeSiImGlc and NpFeSiImMalt) with pore size distribution and pore diameter are shown in Fig. 7. The isotherm results exhibited type IV with hysteresis loop H3-type. The loop was observed in the range of $0.6 < P/P_0 < 1$ for all particles except for the one fabricated with glucose (NpFe-SiImGlc), which shows swelling desorption characteristics. This extended hysteresis loop between the adsorption and desorption curves is not one of the traditional nitrogen isotherm classifications by the international union of pure and applied chemistry (IUPAC).[65] However, the reason could be one of two

either that the pore structure may be changing as a function of the amount adsorbed as reported previously with nanoporous materials[66] or by the influence of plasticizer glycose molecules and their chemical interaction with nitrogen molecules. This effect is clearly seen in the decreased surface area of NpFe-SiImGlc ($\sim$116 m^2 g^{-1}) in comparison to the specific surface area of NpFeSi, NpFeSiIm, and NpFeSiImMalt, which were found to be $\sim$158, 147 and 181, respectively. Also, the average pore volume was influenced by the reduction of the surface site due to immobilization with glucose molecules and their interaction causing overcrowding and thus reduce the porosity size (0.16 cm^3 g^{-1}), while the pore volume for the precursor and particle immobilized with maltose was found to be 0.22, 0.27 and 0.28 cm^3 g^{-1}, respectively. The pore size distribution (figures attached in ESI†) reveals a mesoporous heterogenous pore distribution range of 6.5–8.2 nm.

Nanoparticle interaction with DNA

Due to the pronounced potential of magnetic orientation several research has been decanted to study magnetic nano-particle interaction with biomolecules for a wide range of applications such as diagnosis,[67] tumor therapy,[68] gene therapy,[69] DNA vaccine transfection,[69] biomedicine,[69] data storage,[69] etc. The solid phase DNA extraction is considered as one of the sufficient strategies to isolate and purify DNA. In view of the most recent related study, for example, Mohamad Zandieh and Juewen Liu (2021) designed core–shell MNP coated by polydopamine functionalized with spherical nucleic acids. The main objective of this designed particle was to overcome the DNA extraction without much sequence specificity. In the end, the synthesized particle provides a highly selective DNA extraction.[70] Yalong Bai et al. (2019) reported a modification of MNP with amino, hydroxyl, and carboxyl functional groups for DNA extraction and found that the amino groups have a powerful adsorption capability for DNA with 98% separation rate during DNA extraction without much sequence specificity.[71] Jiuhai Wang et al. (2017) used silica coated MNP for DNA and RNA simultaneous extraction from hepatocellular carcinoma (Hep G2). The average yield obtained for DNA and RNA was high
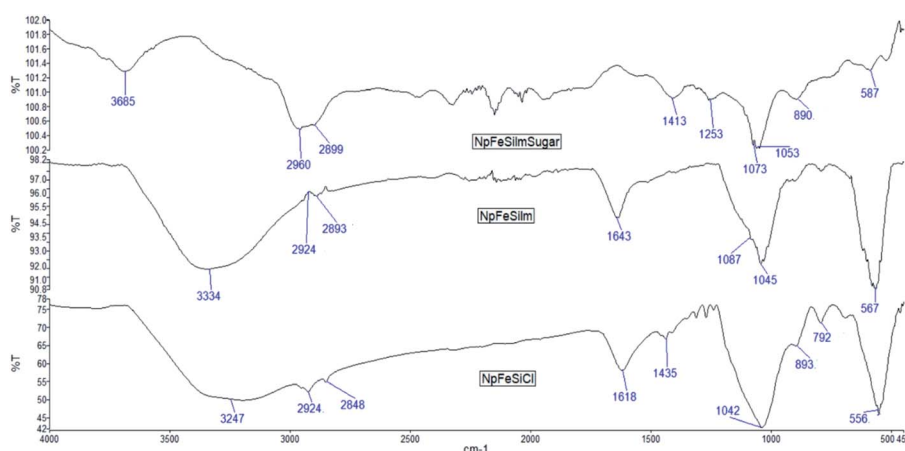

Fig. 6 ATR FT-IR spectra of NpFeSiPrCl, NpFeSiIm, and NpFeSiImSugar.
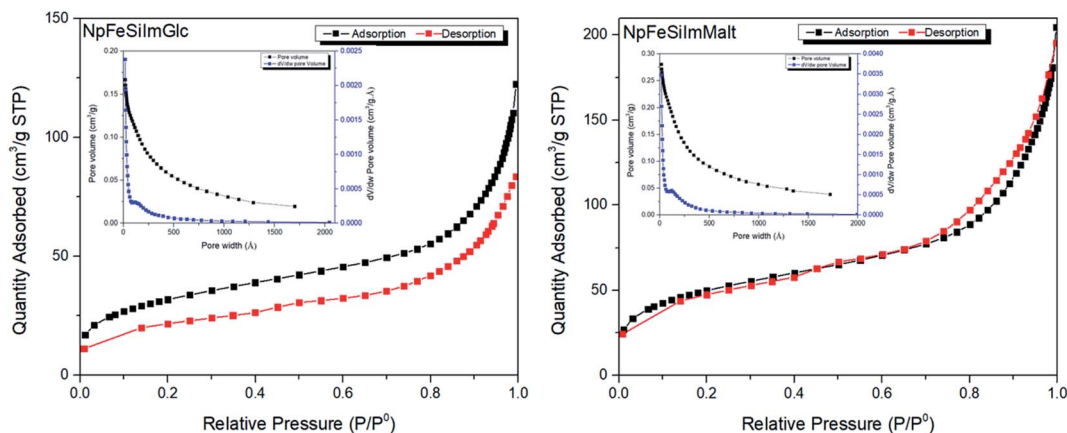
Fig. 7 Nitrogen adsorption–desorption curve of NpFeSiImGlc and NpFeSiImMalt. The inset shows pore volume profile.

(1 mL Hep G2 (~106 cells) that ranged from 9.7 to 14.7 μg with A_{260}/A_{280} values between 1.68 and 2.01) and also reported different optimized factors including lysis buffer, ethanol, MNPs, and washing buffers, which may affect the yield of nucleic acid.[47] Jeong Yu Lee et al. (2017) demonstrated the enhancement delivery of siRNA using ultrasound technique and MNP coated with deoxycholic acid and perfluoropentane as a carrier for successful delivery to lung cancer cells and breast cancer cells. The results show efficient transfection delivery of siRNA without degradation of the molecule, which was able to successfully promote siRNA uptake.[28] Kaijia Xu, et al. (2017) proposed an improved solid-phase extraction of salmon sperm DNA sodium salt by synthesized chitosan-modified Fe_3O_4-magnetized multi-walled carbon nanotubes coated with a poly(ethylene glycol) based deep eutectic solvent. It displays a favorable selectivity for DNA over bovine hemoglobin with isolation of 79% of DNA without conformational damage.[72] Lin Xiong, et al. (2016) reported magnetic core–shell silica nanoparticles functionalized with amnio propyl triethoxy silane to provide amino functional active group with large-pore mesoporous silica. These particles possess both high loading capacity of siRNA (2 wt%) and strong magnetic response. However, the particles significantly enhance the delivery of siRNA to the cancer cells and it was found that the particles coated with tannic acid increase the dispersion stability of the siRNA-loaded carrier and can serve as a pH-responsive releasing switch.[63] Patil, R. M. et al. (2015) investigated the isolation and enrichment of bacterial DNA using MNP with the surface modified with chitosan–glutaraldehyde, and the result was the extracted DNA higher than the usual organic isolation (phenol/chloroform) with better purity of the isolated DNA.[30] However, our main idea was to synthesize a new fabricated magnetic nanoparticle compound with unique properties such as multi-functionality, biodegradable, biocompatible, high product safety, and an environmentally favorable manufacturing process. The new synthesized particles based-sugar performance shows a high desorption rate of DNA (7 min.) with more than 86% of unchanged DNA loading.

The attachment or integration strength of biomolecules such as DNA onto the nanomaterial solid surface plays a crucial role

in the application aspect. Selection of an appropriate immobilization strategy that is suitable for robust reproducibility and operational stability of the transducing is usually preferred in order to prevent desorption of the biomolecules from the solid surface easily. The three different protocols of attachment of DNA to the surface are (i) electrostatic interaction between DNA and a substrate. (ii) Covalent binding of a chemical group attached to the DNA end. (iii) Binding of a protein attached to the DNA end.[73,74] Since the NpFeSiImSugar carries a positive charge, it can electrostatically adsorb DNA, especially with the enhanced properties of the high surface area of the particles, which reduce the distance between the redox sites.[73,74] In addition, the peculiar features of the largest negative charge distribution localized on phosphate groups present on the surface of DNA molecule and in the minor groove[75,51] with electromagnetic properties of particles increasing the interaction and run high as a promising approach to biomolecule extraction. Moreover, the weakly acidic amino groups of DNA act as proton donors in the formation of hydrogen bonds, whereas oxygen atoms of keto groups and nitrogen atoms of heterocyclic bases are proton acceptors,[75] and all of these will provide a strong interaction with particles by oxygen atoms and hydroxyl groups on the sugar molecule.

The adsorption binding of nucleic acids on the surface modified sugar based magnetic particles was investigated in this study with the possibility of separating the complex and recovering the DNA. Fig. 8 clearly shows the magnet attraction capacities of the complex to the external magnetic field.

In order to optimize the interaction condition, the DNA loading capacity was evaluated by agarose gel electrophoresis, as shown in Fig. 9. The investigation was carried out on both mono and di sugar immobilized on magnetic nanoparticles. As NpFeSiImSugar to DNA weight ratio increased from 15 to 60 wt%, the migration of DNA on the gel gradually decreased overall and eventually completely stopped at the weight ratio of 30 and 45 wt% for glycose and maltose fabrication, respectively, which suggested the best combination ability of loading capacity. As mentioned in our previous work, no DNA interaction and loading were observed for precursor (NpFeSi and NpFeSiCl), which proves that the presence of the ionic charge
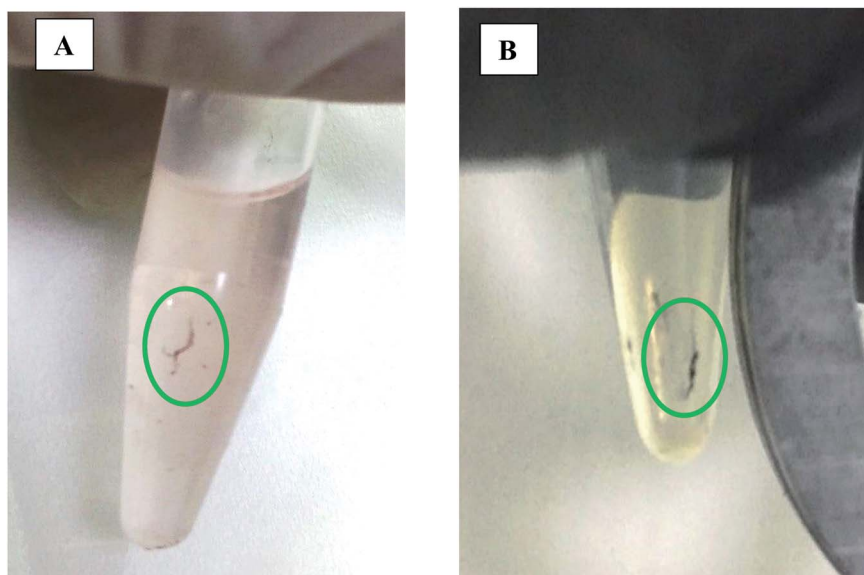
Fig. 8 Pictures illustrating magnet attraction capacities. (A) When nanoparticles attached to DNA particles during DNA extraction process. (B) Nanoparticles–DNA complex in a tube and attraction to magnet are clearly observed.
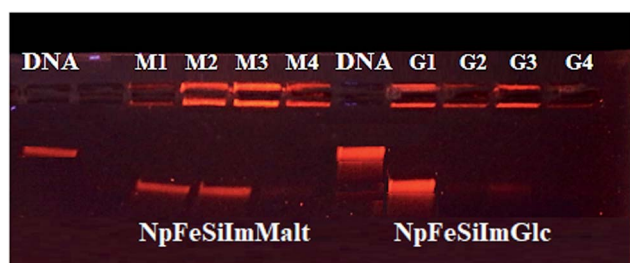

Fig. 9 Gel electrophoresis characterization of DNA conjugates with nanoparticles (NpFeSiImMalt and NpFeSiImGlc) at different weight ratios (wt%) of nanoparticles ranging from 15 to 60. And exposure to the magnetic field. (Lane M) represent DNA–NpFeSiImMalt complex M1 = 15, M2 = 30, M3 = 45, M4 = 60. (Lane G) represent DNA–NpFeSiImGlc complex G1 = 15, G2 = 30, G3 = 45, G4 = 60 with naked DNA.

with multiple hydroxyl molecules plays an important role in the strength of the interaction of the complex.

Fig. 10 shows the gel electrophoresis characterization of DNA–nano complex stability for both sugars at different time periods ranging from 3 h to 4 days. Electrophoretic mobility of DNA in agarose gel was observed with the appearance of a clear band, which indicated that DNA did not undergo any significant degradation with increased time. However, the complex was found to be stable enough even for more than five months without dissociation from the particles when stored at 4 °C.

Since the use of ultrasound has had promising results in improving the delivery and efficacy of therapeutic molecules, the complex of MNP/DNA exposure to ultrasound was mediated for different time ranges of 0–160 s to determine the potential for damaging therapeutic molecules. The agarose gel retardation assay was used to detect any DNA degradation, structural change, and release by breaking the interaction with the particles (Fig. 11). The result was a clear band observed at the same row for the exposed time 5–40 s without any significant change in the DNA, and no effect was observed on MNP/DNA complex interaction. A light drag mark was detected at the exposure time 80–160 s, which comes from the released DNA, but still without affecting their structure. However, these detachment results indicated that the magnetic based sugar nanoparticle did not release the DNA quickly and preserved DNA from degradation,
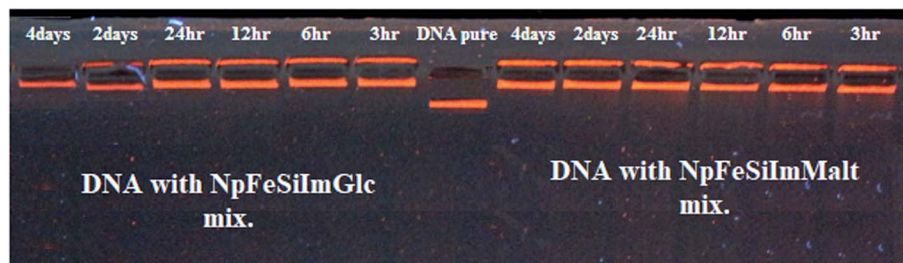

Fig. 10 Gel electrophoresis characterization of DNA stability with nanoparticles (NpFeSiImMalt and NpFeSiImGlc) at different time periods ranging from 3 h to 4 days.
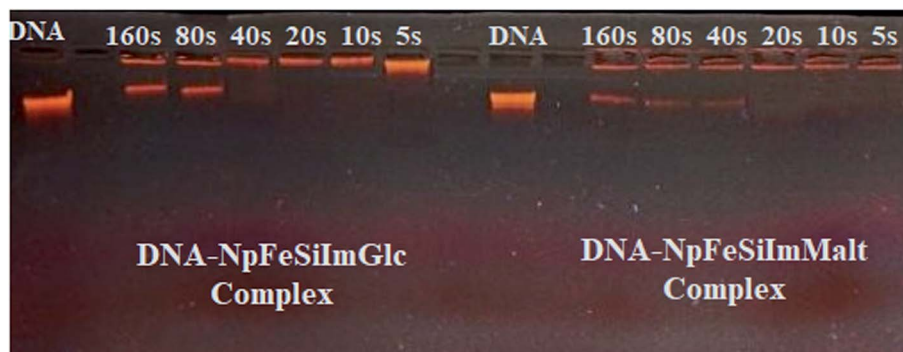
Fig. 11 Gel retardation assay of ultrasound-exposed DNA–MNPs complexes.
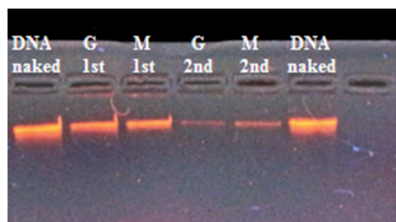

Fig. 12 Electrophoretic DNA profiles for recovering process.

and this is likely to be beneficial for the systemic delivery of medical materials.

The release of DNA from the DNA–nanoparticle complex was carried out to show the possibility of DNA separation and recovery. Fig. 12 shows gel electrophoresis characterization of releasing profile test after disengagement of DNA from DNA–nano complex by using spin column, which contains silica membrane and micro-centrifuge at 14 000 rpm. During the first DNA separation process, without adding elution buffer, a high quantity of DNA was recovered, as shown by a clear band. The second time process was done by adding (50 μL) of elution buffer to the silica membrane, which already contained the DNA–nano complex, and as a result, a tiny amount was observed. This proves that most of the DNA was possibly released the first time easily with a high desorption rate of ~7 min.

Conclusion

In this work, we have designed and synthesized a magnetic core–shell nanoparticle fabricated with imidazolium as a cationic source and carbohydrate molecules as an excellent biocompatible and biodegradable multi-hydroxyl group to provide multi hydrogen bonding. These are targeted for solid phase DNA extraction by reinforcement MNP/DNA complex interaction. In order to prevent the conflict of interaction between the two possible binding sources, a triethylene glycol is used as a spacer between them, as well as to extend the possibility of interaction along the particle surface, and this could also inhibit the solid-state quenching of the particle's interaction. The imidazole and sugar molecules attached to the surface

of MNPs possess the affinity to interact with nucleic acid (NA), which facilitates their rapid, cost-effective, and easy separation by utilizing the proper positioning of an external magnetic field. More importantly, it could even be used for the extraction of small amounts of NA. Overall, this proof of concept might open the door to future therapeutic delivery applications by controlling the delivery and a new generation of carrier materials.

Conflicts of interest

There are no conflicts to declare.

Acknowledgements

References

1 V. Arumugam, K. G. Moodley, A. Dass, R. M. Gengan, D. Ali, S. Alarifi, M. Chandrasekaran and Y. Gao, Ionic liquid covered iron-oxide magnetic nanoparticles decorated zeolite nanocomposite for excellent catalytic reduction and degradation of environmental toxic organic pollutants and dyes, *J. Mol. Liq.*, 2021, **342**, 117492, DOI: **10.1016/j.molliq.2021.117492**.

2 A. M. Abu-Dief and S. M. Abdel-Fatah, Development and functionalization of magnetic nanoparticles as powerful and green catalysts for organic synthesis, *Beni-Suef Univ. J. Basic Appl. Sci.*, 2018, **7**, 55–67, DOI: **10.1016/j.bjbas.2017.05.008**.

3 A. Tufani, A. Qureshi and J. H. Niazi, Iron oxide nanoparticles based magnetic luminescent quantum dots (MQDs) synthesis and biomedical/biological applications: a review, *Mater. Sci. Eng., C*, 2021, **118**, 111545, DOI: **10.1016/j.msec.2020.111545**.

4 F. Ahmadpoor, A. Masood, N. Feliu, W. J. Parak and S. A. Shojaosadati, The Effect of Surface Coating of Iron Oxide Nanoparticles on Magnetic Resonance Imaging

Relaxivity, *Front. Nanotechnol.*, 2021, **3**, 13, DOI: 10.3389/fnano.2021.644734.

5 D. Giuntini, E. Torresani, K. T. Chan, M. Blankenburg, L. Saviot, B. Bor, B. Domènech, M. Shachar, M. Müller, E. A. Olevsky, J. E. Garay and G. A. Schneider, Iron oxide-based nanostructured ceramics with tailored magnetic and mechanical properties: development of mechanically robust{,} bulk superparamagnetic materials, *Nanoscale Adv.*, 2019, **1**, 3139–3150, DOI: 10.1039/C9NA00222G.

6 M. Asgari, M. Soleymani, T. Miri and A. Barati, A robust method for fabrication of monodisperse magnetic mesoporous silica nanoparticles with core-shell structure as anticancer drug carriers, *J. Mol. Liq.*, 2019, **292**, 111367, DOI: 10.1016/j.molliq.2019.111367.

7 S. Laurent, D. Forge, M. Port, A. Roch, C. Robic, L. Vander Elst and R. N. Muller, Magnetic iron oxide nanoparticles: synthesis, stabilization, vectorization, physicochemical characterizations, and biological applications, *Chem. Rev.*, 2008, **108**, 2064–2110, DOI: 10.1021/cr068445e.

8 H. Rui, R. Xing, Z. Xu, Y. Hou, S. Goo and S. Sun, Synthesis, functionalization, and biomedical applications of multifunctional magnetic nanoparticles, *Adv. Mater.*, 2010, **22**, 2729–2742, DOI: 10.1002/adma.201000260.

9 W. Jiang, H. C. Yang, S. Y. Yang, H. E. Horng, J. C. Hung, Y. C. Chen and C.-Y. Hong, Preparation and properties of superparamagnetic nanoparticles with narrow size distribution and biocompatible, *J. Magn. Magn. Mater.*, 2004, **283**, 210–214, DOI: 10.1016/j.jmmm.2004.05.022.

10 D. Chen and R. Xu, Hydrothermal synthesis and characterization of nanocrystalline Fe3O4 powders, *Mater. Res. Bull.*, 1998, **33**, 1015–1021, DOI: 10.1016/S0025-5408(98)00073-7.

11 G. M. da Costa, E. De Grave, P. M. A. de Bakker and R. E. Vandenberghe, Synthesis and Characterization of Some Iron Oxides by Sol-Gel Method, *J. Solid State Chem.*, 1994, **113**, 405–412, DOI: 10.1006/jssc.1994.1388.

12 T. Hyeon, S. S. Lee, J. Park, Y. Chung and H. B. Na, Synthesis of highly crystalline and monodisperse maghemite nanocrystallites without a size-selection process, *J. Am. Chem. Soc.*, 2001, **123**, 12798–12801, DOI: 10.1021/ja016812s.

13 Y. Deng, L. Wang, W. Yang, S. Fu and A. Elaïssari, Preparation of magnetic polymeric particles via inverse microemulsion polymerization process, *J. Magn. Magn. Mater.*, 2003, **257**, 69–78, DOI: 10.1016/S0304-8853(02)00987-3.

14 R. Abu Mukh-Qasem and A. Gedanken, Sonochemical synthesis of stable hydrosol of Fe3O4 nanoparticles, *J. Colloid Interface Sci.*, 2005, **284**, 489–494, DOI: 10.1016/j.jcis.2004.10.073.

15 S. Basak, D.-R. Chen and P. Biswas, Electrospray of ionic precursor solutions to synthesize iron oxide nanoparticles: Modified scaling law, *Chem. Eng. Sci.*, 2007, **62**, 1263–1268, DOI: 10.1016/j.ces.2006.11.029.

16 S. Veintemillas-Verdaguer, M. P. Morales and C. J. Serna, Continuous production of γ-Fe₂O₃ ultrafine powders by laser pyrolysis, *Mater. Lett.*, 1998, **35**, 227–231, DOI: 10.1016/S0167-577X(97)00251-6.

17 Y. Guan, Y. Yang, X. Wang, H. Yuan, Y. Yang, N. Li and C. Ni, Multifunctional Fe3O4@SiO2-CDs magnetic fluorescent nanoparticles as effective carrier of gambogic acid for inhibiting VX2 tumor cells, *J. Mol. Liq.*, 2021, **327**, 114783.

18 N. L. Rosi and C. A. Mirkin, Nanostructures in Biodiagnostics Nathaniel, *Chem. Rev.*, 2005, **105**, 1547–1562.

19 K. Banan, F. Ghorbani-Bidkorbeh, H. Afsharara, D. Hatamabadi, B. Landi, R. Keçili and B. Sellergren, Nano-sized magnetic core-shell and bulk molecularly imprinted polymers for selective extraction of amiodarone from human plasma, *Anal. Chim. Acta*, 2022, **1198**, 339548.

20 L. Qi, T. Dong, X. Jiang, J. Li, B. Di and F. Yan, Preparation of polydopamine-functionalized mesoporous silica-coated core/shell magnetic nanocomposite for efficiently extracting five amphetamine-type stimulants from wastewater followed by UPLC-MS/MS determination, *J. Hazard. Mater.*, 2022, **426**, 128082.

21 W. Lu, S. Fu, X. Sun, J. Liu, D. Zhu, J. Li and L. Chen, Magnetic solid-phase extraction using polydopamine-coated magnetic multiwalled carbon nanotube composites coupled with high performance liquid chromatography for the determination of chlorophenols, *Analyst*, 2021, **146**(20), 6252–6261.

22 A. R. Bagheri, M. Arabi, M. Ghaedi, A. Ostovan, X. Wang, J. Li and L. Chen, Dummy molecularly imprinted polymers based on a green synthesis strategy for magnetic solid-phase extraction of acrylamide in food samples, *Talanta*, 2019, **195**, 390–400.

23 S. Javadian, K. Najafi, S. M. Sadrpoor, F. Ektefa, N. Dalir and M. Nikkhah, Graphene quantum dots based magnetic nanoparticles as a promising delivery system for controlled doxorubicin release, *J. Mol. Liq.*, 2021, **331**, 115746.

24 H. Yang, J. Zhang, Y. Liu, L. Wang, L. Bai, L. Yang, D. Wei, W. Wang, Y. Niu and H. Chen, Rapid removal of anionic dye from water by poly(ionic liquid)-modified magnetic nanoparticles, *J. Mol. Liq.*, 2019, **284**, 383–392.

25 X. Liu, M. A. Fagiry, S. M. Sajadi, R. A. Almasri, A. Karimipour, Z. Li, D. Baleanu and F. Ghaemi, The investigation of Fe₃O₄ atomic aggregation in a nanochannel in the presence of magnetic field: Effects of nanoparticles distance center of mass, temperature and total energy via molecular dynamics approach, *J. Mol. Liq.*, 2022, **384**, 118400.

26 J. Pivetal, G. Ciuta, M. Frenea-robin, N. Haddour, N. M. Dempsey, F. Dumas-bouchiat and P. Simonet, Magnetic nanoparticle DNA labeling for individual bacterial cell detection and recovery, *J. Microbiol. Methods*, 2014, **107**, 84–91.

27 L. Xiong, J. Bi, Y. Tang and S. Z. Qiao, Magnetic Core-Shell Silica Nanoparticles with Large Radial Mesopores for siRNA Delivery, *Small*, 2016, **12**, 4735–4742.

28 J. Y. Lee, C. Crake, B. Teo, D. Carugo, M. de Saint Victor, A. Seth and E. Stride, Ultrasound-Enhanced siRNA Delivery Using Magnetic Nanoparticle-Loaded Chitosan-Deoxycholic Acid Nanodroplets, *Adv. Healthcare Mater.*, 2017, **6**, 1–9.

29 Y. Zhai, Y. A. N. Zhou, X. Li and G. Feng, Immune - enhancing effect of nano - DNA vaccine encoding a gene of

the prME protein of Japanese encephalitis virus and BALB / c mouse granulocyte - macrophage colony - stimulating factor, *Mol. Med. Rep.*, 2015, **12**, 199–209.

30 P. B. Shete, S. M. Patil, S. P. Govindwar and S. H. Pawar, Superparamagnetic Core/Shell Nanostructures for Magnetic Isolation and Enrichment of DNA., *RSC Adv.*, 2015, **5**, 88375–88381.

31 S. Liu and M.-Y. Han, Silica-Coated Metal Nanoparticles, *Chem.–Asian J.*, 2010, **5**, 36–45, DOI: **10.1002/asia.200900228**.

32 V. A. Online, Y. Li and X. Zhong, Highly bright water-soluble silica coated quantum dots with excellent stability, *J. Mater. Chem. B*, 2014, **2**, 5043–5051, DOI: **10.1039/c4tb00458b**.

33 S. Quintana-Sánchez, A. Barrios-Gumiel, J. Sánchez-Nieves, J. L. Copa-Patiño, F. J. de la Mata and R. Gómez, Bacteria capture with magnetic nanoparticles modified with cationic carbosilane dendritic systems, *Mater. Sci. Eng., C*, 2021, 112622, DOI: **10.1016/j.msec.2021.112622**.

34 D. T. Nguyen and K. S. Kim, Controlled magnetic properties of iron oxide-based nanoparticles for smart therapy, *KONA Powder Part. J.*, 2016, **2016**, 33–47, DOI: **10.14356/kona.2016010**.

35 L. Josephson, C. H. Tung, A. Moore and R. Weissleder, High-efficiency intracellular magnetic labeling with novel superparamagnetic-Tat peptide conjugates, *Bioconjugate Chem.*, 1999, **10**, 186–191, DOI: **10.1021/bc980125h**.

36 P. Wunderbaldinger, L. Josephson and R. Weissleder, Crosslinked iron oxides (CLIO): a new platform for the development of targeted MR contrast agents, *Acad. Radiol.*, 2002, **9**(Suppl 2), S304–S306, DOI: **10.1016/s1076-6332(03)80210-6**.

37 K. H. Bae, M. Park, M. J. Do, N. Lee, J. H. Ryu, G. W. Kim, C. Kim, T. G. Park and T. Hyeon, Chitosan oligosaccharide-stabilized ferrimagnetic iron oxide nanocubes for magnetically modulated cancer hyperthermia, *ACS Nano*, 2012, **6**, 5266–5273, DOI: **10.1021/nn301046w**.

38 U. O. Häfeli, J. S. Riffle, L. Harris-Shekhawat, A. Carmichael-Baranauskas, F. Mark, J. P. Dailey and D. Bardenstein, Cell uptake and in vitro toxicity of magnetic nanoparticles suitable for drug delivery, *Mol. Pharm.*, 2009, **6**, 1417–1428, DOI: **10.1021/mp900083m**.

39 M. Mahmoudi, A. Simchi, A. S. Milani and P. Stroeve, Cell toxicity of superparamagnetic iron oxide nanoparticles, *J. Colloid Interface Sci.*, 2009, **336**, 510–518, DOI: **10.1016/j.jcis.2009.04.046**.

40 C. Xu, D. Miranda-Nieves, J. A. Ankrum, M. E. Matthiesen, J. A. Phillips, I. Roes, G. R. Wojtkiewicz, V. Juneja, J. R. Kultima, W. Zhao, P. K. Vemula, C. P. Lin, M. Nahrendorf and J. M. Karp, Tracking mesenchymal stem cells with iron oxide nanoparticle loaded poly(lactide-*co*-glycolide) microparticles, *Nano Lett.*, 2012, **12**, 4131–4139, DOI: **10.1021/nl301658q**.

41 W. Wu, Q. He and C. Jiang, Magnetic iron oxide nanoparticles: synthesis and surface functionalization strategies, *Nanoscale Res. Lett.*, 2008, **3**, 397–415, DOI: **10.1007/s11671-008-9174-9**.

42 Q. Ma, Y. Nakane, Y. Mori, M. Hasegawa, Y. Yoshioka, T. M. Watanabe, K. Gonda, N. Ohuchi and T. Jin, Multilayered, core/shell nanoprobes based on magnetic ferric oxide particles and quantum dots for multimodality imaging of breast cancer tumors, *Biomaterials*, 2012, **33**, 8486–8494, **https://doi.org/10.1016/j.biomaterials.2012.07.051**.

43 K. V Chandekar, M. Shkir, T. Alshahrani, E. H. Ibrahim, M. Kilany, Z. Ahmad, M. A. Manthrammel, S. AlFaify, B. Kateb and A. Kaushik, One-spot fabrication and in vivo toxicity evaluation of core-shell magnetic nanoparticles, *Mater. Sci. Eng., C*, 2021, **122**, 111898, DOI: **10.1016/j.msec.2021.111898**.

44 H. Fatima and K. S. Kim, Magnetic nanoparticles for bioseparation, *Korean J. Chem. Eng.*, 2017, **34**, 589–599, DOI: **10.1007/s11814-016-0349-2**.

45 H. Naeimi and Z. S. Nazifi, A highly efficient nano-Fe₃O₄ encapsulated-silica particles bearing sulfonic acid groups as a solid acid catalyst for synthesis of 1,8-dioxo-octahydroxanthene derivatives, *J. Nanopart. Res.*, 2013, **15**, 2026, DOI: **10.1007/s11051-013-2026-2**.

46 A. Halilu, T. H. Ali, A. Y. Atta, P. Sudarsanam, S. K. Bhargava and S. B. Abd Hamid, Highly Selective Hydrogenation of Biomass-Derived Furfural into Furfuryl Alcohol Using a Novel Magnetic Nanoparticles Catalyst, *Energy Fuels*, 2016, **30**, 2216–2226, DOI: **10.1021/acs.energyfuels.5b02826**.

47 J. Wang, Z. Ali, J. Si, N. Wang, N. He and Z. Li, Simultaneous extraction of DNA and RNA from hepatocellular carcinoma (Hep G2) based on silica-coated magnetic nanoparticles, *J. Nanosci. Nanotechnol.*, 2017, **17**, 802–806, DOI: **10.1166/jnn.2017.12442**.

48 K. Xu, Y. Wang, H. Zhang, Q. Yang, X. Wei and P. Xu, Solid-phase extraction of DNA by using a composite prepared from multiwalled carbon nanotubes, chitosan, Fe₃O₄ and a poly(ethylene glycol)-based deep eutectic solvent, *Microchim. Acta*, 2017, **184**, 4133–4140, DOI: **10.1007/s00604-017-2444-4**.

49 V. L. Dhadge, P. I. Morgado, F. Freitas, M. A. Reis, A. Azevedo, R. Aires-Barros and A. C. A. Roque, An extracellular polymer at the interface of magnetic bioseparations, *J. R. Soc., Interface*, 2014, **11**, 20140743, DOI: **10.1098/rsif.2014.0743**.

50 L.-S. Qing, Y. Xue, W.-L. Deng, X. Liao, X.-M. Xu, B.-G. Li and Y.-M. Liu, Ligand fishing with functionalized magnetic nanoparticles coupled with mass spectrometry for herbal medicine analysis: ligand fishing for herbal medicine analysis, *Anal. Bioanal. Chem.*, 2011, **399**, 1223–1231, DOI: **10.1007/s00216-010-4399-8**.

51 T. H. Ali, A. M. Mandal, T. Heidelberg, R. S. Duali Hussen and E. W. Goh, Ionic magnetic core-shell nanoparticles for DNA extraction, *RSC Adv.*, 2020, **10**, 38818–38830, DOI: **10.1039/d0ra05933a**.

52 C. O. Wilson, J. M. Beale, and J. H. Block, *Wilson and Giswold's Organic Medicinal and Pharmaceutical Chemistry*, Lippincott Williams & Wilkins, Baltimore, MD, 12th edn, 2011.

53 M. G. Roberson, J. M. Duncan, K. J. Flieth, L. M. Geary and M. J. Tucker, Photo-initiated rupture of azobenzene

micelles to enable the spectroscopic analysis of antimicrobial peptide dynamics, *RSC Adv.*, 2020, **10**, 21464–21472, DOI: **10.1039/D0RA01920H**.

54 F. Reise, J. E. Warias, K. Chatterjee, N. R. Krekiehn, O. Magnussen, B. M. Murphy and T. K. Lindhorst, Photoswitchable Glycolipid Mimetics: Synthesis and Photochromic Properties of Glycoazobenzene Amphiphiles, *Chem.–Eur. J.*, 2018, **24**, 17497–17505, DOI: **10.1002/chem.201803112**.

55 T. H. Ali, H. A. B. Tajuddin, R. S. D. Hussen and T. Heidelberg, Increased Emulsion Stability for Reverse Y-Shaped Sugar-Based Surfactants, *J. Surfactants Deterg.*, 2015, **18**, 881–886, DOI: **10.1007/s11743-015-1710-x**.

56 T. H. Ali, R. S. D. Hussen and T. Heidelberg, New Y-shaped surfactants from renewable resources, *Colloids Surf., B*, 2014, **123**, 981–985, DOI: **10.1016/j.colsurfb.2014.10.054**.

57 T. Hussein Ali, R. Syahila Duali Hussen, T. Heidelberg and H. Anua Bin Tajuddin, X-Shaped Sugar-Derived Emulsifiers From 'Click Chemistry' - A New Gemini Surfactant Type for Oil-in-Water Systems, *ChemistrySelect*, 2020, **5**, 6856–6860, DOI: **10.1002/slct.202000929**.

58 T. H. Ali, T. Heidelberg, R. S. D. Hussen and H. A. Tajuddin, Unexpected reactions of terminal alkynes in targeted "click chemistry'' copper-catalyzed azide-alkyne cycloadditions, *Curr. Org. Synth.*, 2019, **16**, 1143–1148, DOI: **10.2174/1570179416666191105152714**.

59 C. Sun, J. S. H. Lee and M. Zhang, Magnetic nanoparticles in MR imaging and drug delivery, *Adv. Drug Delivery Rev.*, 2008, **60**, 1252–1265, DOI: **10.1016/j.addr.2008.03.018**.

60 N. Geerts and E. Eiser, DNA-functionalized colloids: physical properties and applications, *Soft Matter*, 2010, **6**, 4647–4660, DOI: **10.1039/c001603a**.

61 S. B. Primrose and R. M. Twyman, *Principles of Gene Manipulation and Genomics*, Blackwell Publishing, Malden, 7th edn, 2006.

62 Y. Takeno, Y. Murakami, T. Sato, T. Tanigaki, H. S. Park, D. Shindo, R. M. Ferguson and K. M. Krishnan, Morphology and magnetic flux distribution in superparamagnetic, single-crystalline Fe_3O_4 nanoparticle rings, *Appl. Phys. Lett.*, 2014, **105**, 5, DOI: **10.1063/1.4901008**.

63 L. Xiong, J. Bi, Y. Tang and S. Z. Qiao, Magnetic Core-Shell Silica Nanoparticles with Large Radial Mesopores for siRNA Delivery, *Small*, 2016, **12**, 4735–4742, DOI: **10.1002/smll.201600531**.

64 J. Ge, Y. Hu, M. Biasini, W. P. Beyermann and Y. Yin, Superparamagnetic magnetite colloidal nanocrystal clusters, *Angew. Chem., Int. Ed.*, 2007, **46**, 4342–4345, DOI: **10.1007/s10951-010-0189-6**.

65 F. Rouquerol, J. Rouquerol, K. S. W. Sing, P. Llewellyn, and G. Maurin, *Adsorption by Powders and Porous Solids:*

Principles, Methodology and Applications, Academic Press, Cambridge, MA, 2013.

66 J. C. Schaeperkoetter, M. J. Connolly, Z. N. Buck, H. Taub, H. Kaiser and C. Wexler, Adsorption-Induced Expansion of Graphene Oxide Frameworks: Observation by In Situ Neutron Diffraction, *ACS Omega*, 2019, **4**, 18668–18676, DOI: **10.1021/acsomega.9b02589**.

67 J.-Y. Lin and Y.-C. Chen, Functional magnetic nanoparticle-based trapping and sensing approaches for label-free fluorescence detection of DNA, *Talanta*, 2011, **86**, 200–207, DOI: **10.1016/j.talanta.2011.08.061**.

68 M. Yin, Z. Li, Z. Liu, J. Ren, X. Yang and X. Qu, Photosensitizer-incorporated G-quadruplex DNA-functionalized magnetofluorescent nanoparticles for targeted magnetic resonance/fluorescence multimodal imaging and subsequent photodynamic therapy of cancer, *Chem. Commun.*, 2012, **48**, 6556–6558, DOI: **10.1039/C2CC32129G**.

69 Y. Namiki, T. Namiki, H. Yoshida, Y. Ishii, A. Tsubota, S. Koido, K. Nariai, M. Mitsunaga, S. Yanagisawa, H. Kashiwagi, Y. Mabashi, Y. Yumoto, S. Hoshina, K. Fujise and N. Tada, A novel magnetic crystal-lipid nanostructure for magnetically guided in vivo gene delivery, *Nat. Nanotechnol.*, 2009, **4**, 598–606, DOI: **10.1038/nnano.2009.202**.

70 M. Zandieh and J. Liu, Spherical Nucleic Acid Mediated Functionalization of Polydopamine-Coated Nanoparticles for Selective DNA Extraction and Detection, *Bioconjugate Chem.*, 2021, **32**, 801–809, DOI: **10.1021/acs.bioconjchem.1c00078**.

71 Y. Bai, D. Roncancio, Y. Suo, Y. Shao, D. Zhang and C. Zhou, A method based on amino-modified magnetic nanoparticles to extract DNA for PCR-based analysis, *Colloids Surf., B*, 2019, **179**, 87–93, DOI: **10.1016/j.colsurfb.2019.03.005**.

72 K. Xu, Y. Wang, H. Zhang, Q. Yang, X. Wei, P. Xu and Y. Zhou, Solid-phase extraction of DNA by using a composite prepared from multiwalled carbon nanotubes, chitosan, Fe_3O_4 and a poly(ethylene glycol)-based deep eutectic solvent, *Microchim. Acta*, 2017, **184**, 4133–4140, DOI: **10.1007/s00604-017-2444-4**.

73 K. M. Abu-Salah, A. A. Ansari and S. A. Alrokayan, DNA-based applications in nanobiotechnology, *J. Biomed. Biotechnol.*, 2010, **2010**, 715295.

74 K. M. Abu-Salah, S. A. Alrokyan, M. N. Khan and A. A. Ansari, Nanomaterials as analytical tools for genosensors, *Sensors*, 2010, **10**, 963–993, DOI: **10.3390/s100100963**.

75 A. G. Pershina, A. E. Sazonov and V. D. Filimonov, Magnetic nanoparticles–DNA interactions: design and applications of nanobiohybrid systems, *Russ. Chem. Rev.*, 2014, **83**, 299–322, DOI: **10.1070/rc2014v083n04abeh004412**.